Ecotoxicology and Environmental Safety 239 (2022) 113672

Contents lists available at ScienceDirect

Ecotoxicology and Environmental Safety

journal homepage: www.elsevier.com/locate/ecoenv

Fluoride exposure induces lysosomal dysfunction unveiled by an integrated transcriptomic and metabolomic study in bone marrow mesenchymal stem cells

Hui Wang [a,1], Lu Yang [b,1], Peng Gao [a,1], Ping Deng [a], Yang Yue [a], Li Tian [a], Jia Xie [a], Mengyan Chen [a], Yan Luo [a], Yidan Liang [c], Weijia Qing [a,d], Zhou Zhou [e], Huifeng Pi [a,*], Zhengping Yu [a,*]

[a] Department of Occupational Health (Key Laboratory of Electromagnetic Radiation Protection, Ministry of Education), Third Military Medical University, Chongqing, China
[b] Hunan Province Prevention and Treatment Hospital for Occupational Diseases, Hunan, China
[c] School of Medicine, Guangxi University, Nanning, Guangxi Zhuang Autonomous Region, China
[d] The 63710th Military Hospital of PLA, Xinzhou, Shanxi, China
[e] Department of Environmental Medicine, School of Public Health, and Department of Emergency Medicine, First Affiliated Hospital, School of Medicine, Zhejiang University, Hangzhou, Zhejiang, China

ARTICLE INFO

Edited by: Professor Bing Yan

Keywords:
Fluoride
Bone marrow mesenchymal stem cells
Lysosome
Transcriptomic
Metabolomic

ABSTRACT

Fluoride has received much attention for its predominant bone toxicity in the human body. However, the toxic mechanism of bone injury caused by fluoride exposure remains largely unclear. Bone marrow mesenchymal stem cells (BMSCs) are widely used as model cells for evaluating bone toxicity after environmental toxicant exposure. In this study, BMSCs were exposed to fluoride at 1, 2, and 4 mM for 24 h, and fluoride significantly inhibited cell viability at 2 and 4 mM. A multiomics analysis combining transcriptomics with metabolomics was employed to detect alterations in genes and metabolites in BMSCs treated with 2 mM fluoride. Kyoto Encyclopedia of Genes and Genomes (KEGG) pathway analysis of transcriptomics profiles identified "lysosomes" as the top enriched pathway, which was severely damaged by fluoride exposure. Lysosomal damage was indicated by decreases in the expression of lysosomal associated membrane protein 2 (LAMP 2) and cathepsin B (CTSB) as well as an increase in pH. Upregulation of the lysosome-related genes *Atp6v0b* and *Gla* was observed, which may be attributed to a compensatory lysosomal biogenesis transcriptional response. Interestingly, inhibition of glutathione metabolism was observed in fluoride-treated BMSCs at the metabolomic level. Moreover, an integrative analysis between altered genes, metabolites and lysosome signaling pathways was conducted. Palmitic acid, prostaglandin C2, and prostaglandin B2 metabolites were positively associated with *Atp6v0b*, a lysosome-related gene. Overall, our results provide novel insights into the mechanism responsible for fluoride-induced bone toxicity.

1. Introduction

Fluorine is a ubiquitous element worldwide and has been detected in human urine and blood samples (Cui et al., 2018; Malin et al., 2018; Liu et al., 2020a, 2020b; Wang et al., 2020a, 2020b). The World Health Organization (2004) regulated the upper limit of 1.5 mg/L fluoride in

Abbreviations: BMSCs, bone marrow mesenchymal stem cells; CTSB, cathepsin B; CTSD, cathepsin D, DAMs, differentially abundant metabolites; DEGs, differentially expressed genes; ECM, extracellular matrix; ER, endoplasmic reticulum; GO, Gene Ontology; KEGG, Kyoto Encyclopedia of Genes and Genomes; LAMP 1, lysosomal associated membrane protein 1; LAMP 2, lysosomal associated membrane protein 2; LC-MS, liquid chromatography-mass spectrometry; OPLS-DA, orthogonal projections to latent structures-discriminate analysis; PCA, principal component analysis; PLS-DA, partial least squares-discrimination analysis; ROS, reactive oxygen species; TFEB, transcription factor EB; V-ATPase, vacuolar H+-ATPase.

* Corresponding authors.
E-mail addresses: pihuifeng2010@163.com, pihuifeng@tmmu.edu.cn (H. Pi), yuzping_tmmu@126.com (Z. Yu).
[1] These authors contributed equally to this work

https://doi.org/10.1016/j.ecoenv.2022.113672
Received 4 February 2022; Received in revised form 13 May 2022; Accepted 18 May 2022
Available online 24 May 2022

drinking water (Helte et al., 2021; Khattak et al., 2022). However, the actual intake of fluoride by approximately 260 million people across the globe is higher than the limit (Rashid and Bezbaruah, 2020; Rashid et al., 2021). Because fluoride has been widely applied in industrial processes, including fossil combustion, fertilizer production, electroplating, glass and ceramic production, high levels of fluoride are detected in soil, water and the atmosphere (Affonso et al., 2020; Han et al., 2021; Li et al., 2021a, 2021b, 2021c, 2021d). Fluoride pollution inevitably results in its transfer into plants, animals, and the human body (Singh et al., 2018; Li et al., 2021a, 2021b, 2021c, 2021d; Liu et al., 2021a, 2021b). It has been reported that excessive fluoride intake caused muti-organ toxicity in bones, teeth, liver, kidney, brain, and gonads in humans (Zhao et al., 2019; Wang et al., 2020b; Meena and Gupta, 2021). Due to its strong bone affinity, the majority of fluoride accumulates in calcified tissues in adults and leads to skeletal fluorosis, which is manifested by osteosclerosis, bone deformations and osteoporosis (Yu et al., 2021; Solanki et al., 2022). Importantly, skeletal fluorosis remains irreversible and endemic in more than 25 countries worldwide. Effective protective and therapeutic measures are still lacking (Ebrahim et al., 2019; Shankar et al., 2021). Therefore, skeletal fluorosis is still a severe threat to global public health and requires further investigation.

In recent studies, excessive fluoride exposure has been shown to activate the PI3K/Akt signaling pathway, thereby leading to excessive proliferation and differentiation of osteoblasts and triggering osteosclerotic skeletal fluorosis *in vivo*. An experiment was conducted to demonstrate that long-term exposure to fluoride inhibited the development of chondrocytes and led to apoptosis in ducks (Wang et al., 2021). In addition, studies revealed that the suppression of transforming growth factor-beta receptor 2 (TGFBR2) and Smad3, mediated by fluoride-induced hyper H3K9 trimethylation, was related to the skeletal fluorosis process (Wei et al., 2019). However, the molecular mechanisms by which fluoride exposure induces bone toxicity are not sufficiently defined.

Bone marrow mesenchymal stem cells (BMSCs), a kind of stem cell mainly isolated from bone marrow, can differentiate into a series of functional somatic cells, such as osteoblasts, chondrocytes, adipocytes and myocardial cells, making it critical for the formation and regeneration of bones (Lu et al., 2019). Thus, BMSCs have been widely used for bone toxicity studies on hazardous substances to investigate their harmful effects on human health and explore the detailed toxicological mechanism. In our previous studies, cadmium (Cd) induced BMSC autophagic cell death by activating the nuclear translocation of FOXO3a or transcription factor E3 (TFE3), contributing to Cd-mediated bone toxicity (Yang et al., 2016; Pi et al., 2019). Alcohol blocked osteogenic differentiation by inhibiting the PTEN/Akt pathway in BMSCs, which may be involved in alcohol-induced bone injury (Chen et al., 2019). Moreover, BMSCs were exposed to irradiation for 12 weeks, and the ratio of Runx2/PPARγ was sharply decreased compared to that in the control group, demonstrating that long-term irradiation partially triggered BMSC-mediated bone loss and increased the bone fracture risk (Zou et al., 2016). Conspicuously, fluoride also inhibited osteogenic processes related to BMSC apoptosis (Zhang et al., 2019). Overall, the results from numerous previous studies suggest that BMSCs represent a valuable *in vitro* model to investigate the mechanism of fluoride-induced bone toxicity.

With the rapid advances in high-throughput methods, omics techniques have become efficient tools in toxicology research. Transcriptomic profiling is utilized to reveal signaling pathways in response to toxicant exposure at the transcriptional level and identify valuable biomarkers in biological processes (Geng et al., 2019). Metabolomics, a comprehensive profiling of the small-molecule metabolites in various biosystems, helps to clarify the effect of various biomarkers involved in biological processes as well as toxicity mechanisms (Hao et al., 2019). Furthermore, the integration of transcriptomics and metabolomics provides a system-wide understanding of the genetic and metabolomic alterations associated with cellular physiology processes influenced by environmental factors (Qiao et al., 2021). Thus, the present study aimed to elucidate the profiles of gene and metabolite reprogramming in fluoride-exposed BMSCs. The findings from this study provided novel insights into the biological mechanisms of fluoride-induced bone toxicity.

2. Materials and methods

2.1. Chemicals and reagents

Sodium fluoride (NaF, A10225-500 g) was purchased from Xiya Reagent (Shandong, China). Stock solutions were prepared in water, stored at room temperature and diluted in fresh medium when used.

2.2. Cell culture

C57BL/6J mouse BMSCs were purchased from Cyagen Biosciences (Guangzhou, China, MUBMX-01001). The BMSCs were cultured in Dulbecco's high-glucose modified Eagle's medium (DMEM) (Sigma, D629) supplemented with 10% FBS (Biological Industries, 04-001-1 A) and 1% penicillin/streptomycin (Gibco, 15,140-122). The BMSCs were incubated at 37 °C in a 5% CO2 humidified atmosphere.

2.3. Cell viability

BMSCs were seeded in 96-well plates at a density of 4000 cells per well and cultured overnight. Then, the BMSCs were treated with fluoride at concentrations of 0, 1, 2, and 4 mM for 24 h, and cell viability was measured by a cell counting kit-8 assay (Dojindo, Japan, CK04). Then, the OD value was measured at 450 nm by a microplate reader (Infinite M200, Tecan, Switzerland).

2.4. Cytotoxicity assays

The IncuCyte ZOOM Live Cell Analysis System (Essen BioScience, USA) was used for continuous monitoring of BMSC survival and proliferation after fluoride treatment. Cells were seeded at 4000 cells/well in 96-well plates and cultured overnight. Then, the cells were treated with fluoride at concentrations of 0, 1, 2, and 4 mM. Subsequently, the plates were scanned, and phase-contrast images were acquired in real time every 8 h from 0 to 24 h after treatment. The confluence per well at each time point was calculated by IncuCyte ZOOM software (Deng et al., 2021).

2.5. Transcriptome analysis

Total RNA extraction was performed according to a previous study (Yue et al., 2021). Briefly, BMSCs were cultured overnight and treated with fluoride at 0 or 2 mM for 24 h. Then, total RNA was extracted from BMSCs with RNAiso Plus (Takara, 9109). Then, sequencing of total RNA was performed by BioNovoGene (Jiangsu, China), and 6 samples, including three pairs of control and fluoride-treated groups, were sequenced. Furthermore, the RNA concentration was monitored on 1% agarose gels and an Agilent 2100 Bioanalyzer, and the mRNA with a polyA structure in the total RNA was enriched by Oligo (dT) magnetic beads. Moreover, the RNA was fragmented to a length of approximately 300 bp, and the RNA fragment was amplified by PCR to approximately 450 bp. Next, the library quality was evaluated on an Agilent 2100 Bioanalyzer. Finally, next-generation sequencing (NGS) was used to pair-end these libraries based on the Illumina sequencing platform.

The clean reads with removed low-quality original reads were mapped to the reference genome using HISAT2 (http://ccb.jhu.edu/software/hisat2/index.shtml). Then, HTSeq software (v 1.99.2) was used to quantify gene expression levels, and the differentially expressed genes (DEGs) between the fluoride treatment group and the control

group were compared. FPKM was applied to standardize the gene expression level, and a FPKM value >1 indicated valid expression. The R Programming Language DESeq software (v 3.14) was used to identify DEGs with the cutoff criteria of $|\log_2$ fold change$| > 1$ and $p < 0.05$. Volcano plots were drawn to show the overall distribution of DEGs in the control and fluoride-treated groups, presented as red and blue dots by Ggplots2 software (v 3.3.5). TopGO (v 2.14.0) was used to visualize the Gene Ontology (GO) enrichment results and to analyze the results with a variety of statistical methods.

2.6. Immunocytochemical analysis

Immunocytochemistry assays were performed as previously reported (Pi et al., 2019b). Briefly, BMSCs were cultured on coverslips overnight at a density of 1.5×10^4 cells per piece, and the cells were then treated with 0, 1, 2 and 4 mM fluoride for 24 h. Next, the cells were fixed with 4% paraformaldehyde (Sigma, 16,005) for 15 min after being washed with PBS three times. After that, the cells were permeabilized with 0.25% Triton X-100 for 15 min. The cells were blocked with goat serum (zsbio, ZLI-9022) for 30 min at room temperature and incubated with anti-CTSB (1:100, Invitrogen, PA5-47975) and anti-CTSD (1:100, Invitrogen, MA5-32127) antibodies overnight at 4 ℃. The cells were then rinsed and incubated with appropriate Alexa Fluor 568 secondary antibodies (1:200, Life Technologies, A10042) for 1 h at room temperature followed by washing with PBST solution 3 times. The cells were then counterstained with DAPI Staining Solution (Beyotime, C1005) for 5 min and sealed with antifade fluorescence mounting medium (Beyotime, P0126). The stained samples were observed by a Zeiss confocal laser scanning microscope (Zeiss, LSM780), and quantitative analysis was performed using ImageJ software (v 1.8.0).

2.7. LysoSensor green staining

After the BMSCs were treated with fluoride at different concentrations of 0, 1, 2, and 4 mM for 24 h, the cells were incubated with 1 μM LysoSensor Green DND-189 (Invitrogen, L7535) for 5 min at 37 °C. Then, the cells were washed 3 times with PBS, and the fluorescence intensity was determined by a Zeiss confocal laser scanning microscope (Zeiss, LSM780). Quantitative analysis was performed using ImageJ software (v 1.8.0).

2.8. Measurement of reactive oxygen species (ROS) levels

Intracellular ROS generation was measured by 5,6-chloromethyl-2′,7′-dichlorodihydrofluorescein diacetate (CM-H2DCFDA; Molecular Probes, C6827). The cells (4000/well) were plated in 96-well black plates and treated with 0, 1, 2, and 4 mM fluoride for 24 h. Then, the cells were incubated with 25 μM CM-H2DCFDA for 30 min at 37°C. The cells were then washed twice with Hanks' balanced salt solution (HBSS) (Beyotime, C0218). After treatment, the fluorescence intensity of the cells was quantified using an Infinite™ M200 Microplate Reader with 485-nm excitation and 538-nm emission filters.

2.9. Quantitative real-time PCR (qRT–PCR)

Quantitative real-time PCR was performed as described previously (Liu et al., 2021a, 2021b). Briefly, total RNA was isolated from BMSC samples using RNAiso Plus (Takara, 9109) and reverse-transcribed using a PrimeScript RT Reagent Kit with gDNA Eraser (Perfect Real Time; TaKaRa, RR047A). Real-time PCR was performed with a Bio–Rad CFX96 Detection System with SYBR Master Mix (Bio–Rad, USA). The primer sequences are listed in Table S1.

2.10. Metabolite extraction

A total of 100 μL of the whole target sample was mixed with 400 μL of acetonitrile: methanol: ddH_2O (2:2:1, V: V: V), vortexed for 30 s, immersed in liquid nitrogen for 5 min, frozen at room temperature, and then centrifuged at 12000 rpm and 4 ℃ for 10 min. The supernatant was mixed with 100 μL of acetonitrile:0.1% FA (1:9, V: V) solution (without 2-chlorophenylalanine). Quality control (QC) analysis was applied to correct the deviation caused by the sample or test system. After filtration on a 0.22 μM membrane, the samples were prepared for liquid chromatography–mass spectrometry (LC-MS) detection. Chromatographic separation was performed on an ACQUITY UPLC® HSS T3 column (150×2.1 mm, 1.8 μm, Waters) maintained at 40 ℃. Gradient elution of analytes was carried out with 0.1% formic acid in water (C) and 0.1% formic acid in acetonitrile (D) or with 5 mM ammonium formate in water (A) and acetonitrile (B) at a flow rate of 0.25 mL/min. After equilibration, 2 μL of each sample was injected. An increasing linear gradient of solvent B (v/v) was applied as follows: 0-1 min, 2% B/D; 1-9 min, 2%-50% B/D; 9-12 min, 50%-98% B/D; 12-13.5 min, 98% B/D; 13.5-14 min, 98%-2% B/D; and 14-20 min, 2% D-positive model (14-17 min, 2% B-negative model). The temperature of the autosampler was 8 ℃. The ESI-MSn experiments were performed according to a previous study (Monnerat et al., 2018; Abdelhafez et al., 2020).

2.11. Liquid chromatography–mass spectrometry (LC/MS)

ProteoWizard software (v3.0.8789) was applied to convert the raw data into the MzXML format. The XCMS Package of R (v 3.3.2) was applied for peak identification, peak filtration, and peak alignment and to obtain a data matrix including the mass-to-charge ratio (m/z), retention time (rt) and intensity information. Multivariate statistical analysis, including principal component analysis (PCA), partial least squares discriminant analysis (PLS-DA), and orthogonal partial least squares discriminant analysis (OPLS-DA), were performed using SIMCA-P (v 13.0). In OPLS-DA, the VIP > 1 and $p < 0.05$ determined using one-way ANOVA or $p < 0.05$ determined using two-way ANOVA were the criteria for determining significance.

2.12. Enrichment, pathway and network analyses of the transcriptome and metabolome

In this study, the DEGs and differentially abundant metabolites (DAMs) were used for enrichment and pathway analysis of the GO (http://bioinfo.cau.edu.cn/agriGO/) and KEGG (https://www. kegg.jp/kegg/pathway.htmL) results. To analyze the relationships between DEGs and DAMs in BMSCs under fluoride treatments, the DEGs and DAMs were mapped to the KEGG pathway data to construct a heatmap for the correlation analysis. Finally, the integrated network analysis of DEGs and DAMs was performed using Cytoscape software (v 3.1.1).

2.13. Statistics

All data are expressed as the mean ± SEM, and each experiment was performed at least three times. Statistical analysis was performed in GraphPad Prism 8.0 (GraphPad software, USA), and the 2-tailed Student's t test or one-way ANOVA followed by Dunn's post-hoc test was performed. $P < 0.05$ was considered statistically significant.

3. Results

3.1. Fluoride treatment inhibited BMSC proliferation

We assessed the toxic effect of fluoride exposure on BMSC proliferation for 24 h and the half maximal inhibitory concentration (IC_{50}) was calculated to be 2.795 mM (Fig. 1A), and the survival rate of BMSCs was significantly reduced after 2 and 4 mM fluoride treatment for 24 h (Fig. 1B). Then, we used an IncuCyteZOOM system to observe the morphology of BMSCs exposed to fluoride at various doses for 0, 8, 16, and 24 h *in vitro*. As shown in Figs. 1C and 1D, cell confluence was

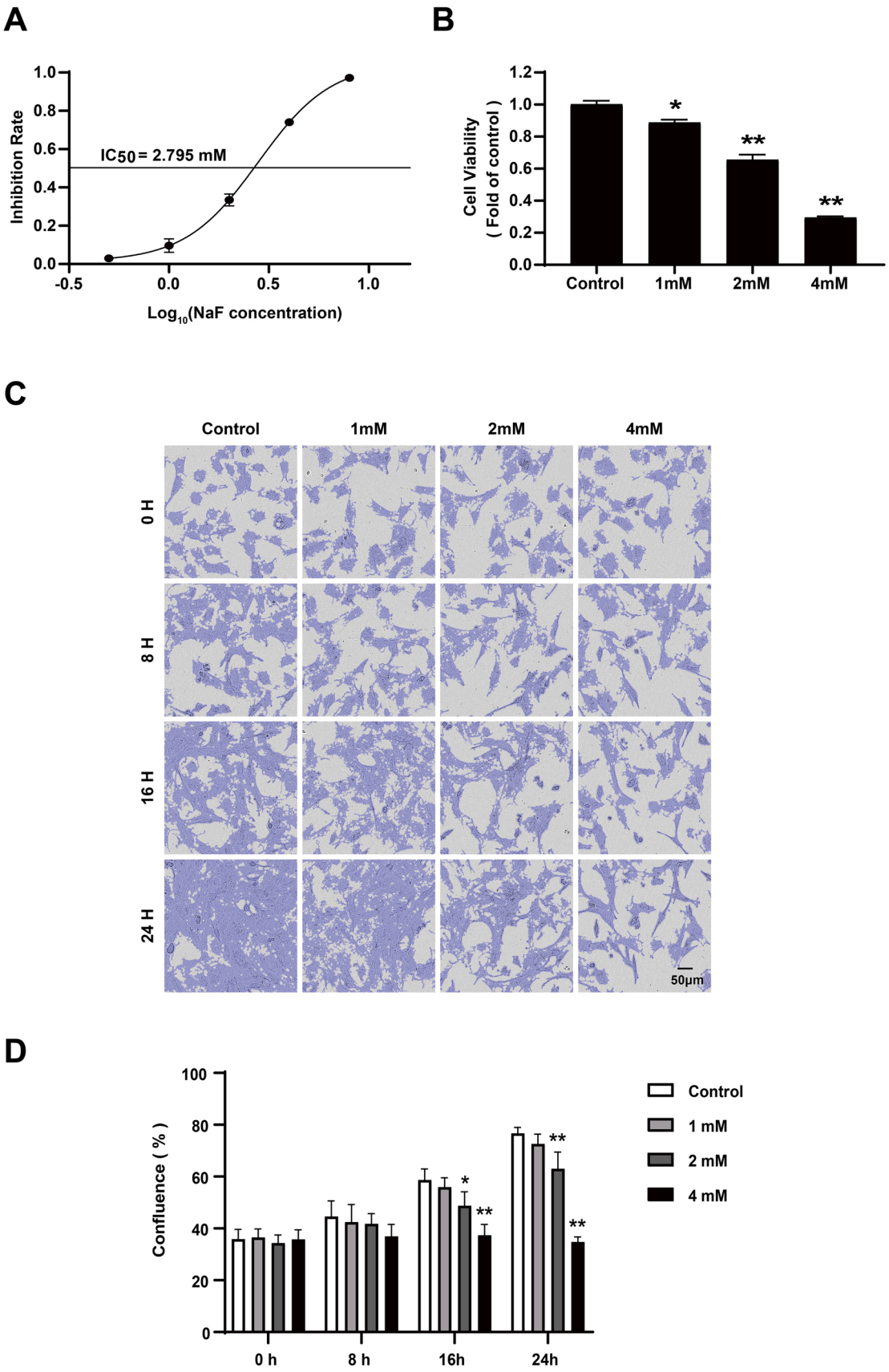

Fig. 1. Fluoride exposure inhibited the viability of BMSCs. (A-B) The IC_{50} values and viability of BMSCs treated with fluoride at different concentrations for 24 h were determined using a CCK-8 assay. (C-D) Alterations in the morphology and confluence of BMSCs treated with fluoride at different concentrations (0, 1, 2, and 4 mM) for 0 h, 8 h, 16 h or 24 h were observed. The values are presented as the means ± SEM. * $p < 0.05$ and ** $p < 0.01$ versus the control group (n = 4).

significantly decreased after 2 and 4 mM fluoride treatment for 16 h and 24 h. Overall, these results indicated that fluoride reduced BMSC proliferation in a concentration- and time-dependent manner.

3.2. Transcriptomic profiling analysis of fluoride-treated BMSCs

To illustrate the underlying mechanisms and related molecular events of fluoride toxicity in BMSCs, RNA-seq-based transcriptome analysis was used to identify DEGs after 2 mM fluoride treatment. The PCA results showed obvious variations in the transcripts between the control group and the 2 mM fluoride-treated group (Fig. 2A). Compared to the control group, a total of 165 upregulated genes and 32 downregulated genes in the fluoride-treated group were detected, and the criteria of $p < 0.05$ and a fold change cutoff criterion > 2 were assigned

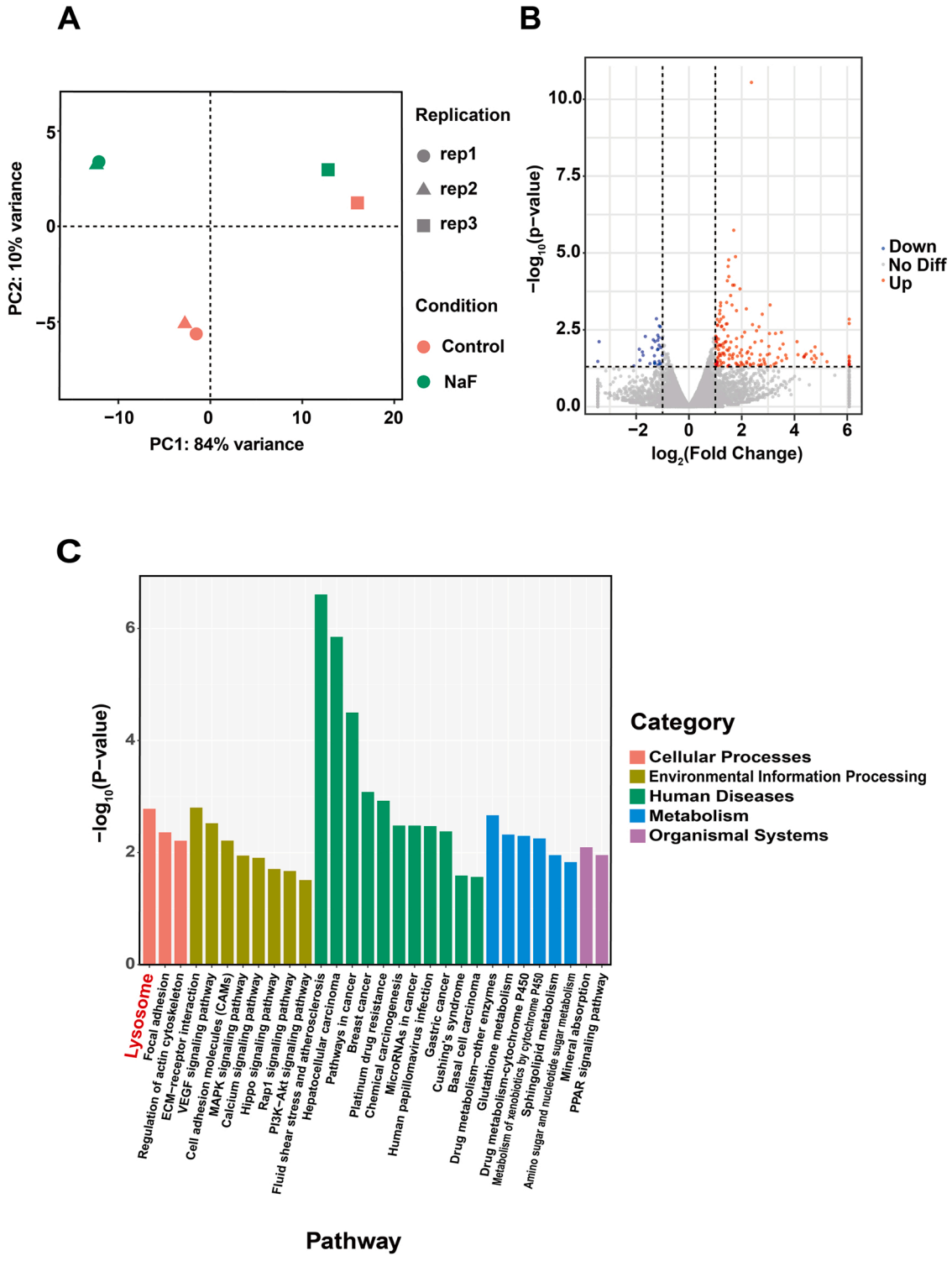

Fig. 2. "Lysosome" was the top enriched KEGG signaling pathway in the transcriptomics data. (A) PCA score plot of the transcriptomic profile in the control and 2 mM fluoride-treated groups. (B) Volcano plots of DEGs between the control group and the 2 mM fluoride-exposed group. (C) Top 20 enriched KEGG signaling pathways.

as significant changes (Fig. 2B). To explore biological process alterations in fluoride-exposed BMSCs, we conducted a pathway-based analysis by applying the KEGG database ($p < 0.05$). The KEGG database revealed that the DEGs were involved in numerous biological processes in organismal systems, including lysosome, focal adhesion, and regulation of actin cytoskeleton in cellular processes, extracellular matrix (ECM)-receptor interactions, VEGF signaling, cell adhesion molecules (CAMs), MAPK signaling, calcium signaling, Hippo signaling, Rap1 signaling, and PI3K-Akt signaling in environmental information processing, fluid shear stress and atherosclerosis, hepatocellular carcinoma, pathways in cancer, breast cancer, platinum drug resistance, chemical carcinogenesis, microRNAs in cancer, human papillomavirus infection, gastric cancer, Cushing's syndrome, basal cell carcinoma in human diseases, drug metabolism-other enzymes, glutathione metabolism, drug metabolism-cytochrome P450, metabolism of xenobiotics by cytochrome P450, sphingolipid metabolism, amino sugar and nucleotide sugar metabolism, mineral absorption and PPAR signaling (Fig. 2C).

3.3. Fluoride treatment impaired lysosomal function in BMSCs

The lysosomal pathway functions in transport and catabolism in the cell. Because this pathway was the top enriched pathway identified in the KEGG analysis, we determined whether fluoride inhibited the lysosomal function of BMSCs. After the BMSCs were treated with fluoride at 1, 2 and 4 mM for 24 h, we performed RT-qPCR to determine the relative mRNA levels of the *LAMP 1* and *LAMP 2* genes, which play crucial roles in maintaining the structural integrity of the lysosomal compartment. Although the *LAMP 1* gene was upregulated, the *LAMP 2* gene was downregulated, indicating that lysosomal membrane integrality was impaired by 2 and 4 mM fluoride (Fig. 3A-B). Moreover, the lysosomal pH variation was evaluated using LysoSensor^{TM} Green DND-189 staining, and we found that fluoride at 2 and 4 mM significantly decreased the LysoSensor signal and increased the lysosomal pH (Fig. 3C and D). Cathepsin B (CTSB) and cathepsin D (CTSD) are major proteolytic enzymes in lysosomes and are involved in protein degradation in physiological and pathological processes. After 2 and 4 mM fluoride treatment, the CTSB fluorescence signal, but not the CTSD signal, was obviously decreased compared to that in the control group (Fig. 3E-F and Fig. S1). Overall, these results indicated that fluoride perturbed the lysosomal function of BMSCs by disrupting lysosomal structural integrity and acidifying the lysosomal compartment.

3.4. Fluoride treatment increased the expression of lysosomal-related genes in BMSCs

We then performed RT–qPCR to detect the relative mRNA levels of the *Atp6v0b, Gla, Neu1*, *Gnptg*, *Idua* and *Mcoln1* genes related to the lysosomal pathway that were identified in the KEGG analysis of transcriptome data (Fig. 4A). The relative *Atp6v0b* and *Gla* mRNA levels were significantly upregulated in BMSCs treated with 2 and 4 mM fluoride compared to the control group (Fig. 4B and E), whereas the *Neu1*, *Gnptg*, *Idua* and *Mcoln1* mRNA levels were significantly upregulated in the 4 mM fluoride treatment group compared to the control group (Fig. 4C-D and F-G). These results suggested that treatment with 2 mM fluoride disturbed lysosomal function and upregulated the expression of the *Atp6v0b* and *Gla* genes. These two genes encode a component of vacuolar H^+-ATPase (V-ATPase) that mediates lysosomal acidification and a homodimeric glycoprotein that hydrolyses the terminal α-galactosyl moieties from glycolipids and glycoproteins, respectively.

3.5. Fluoride treatment disturbed BMSC metabolism

To explore the differences in perturbed metabolites and metabolic pathways in BMSCs between the 2 mM fluoride-treated group and the control group, LC/MS was applied to produce reliable metabolomic data with definitive strong signals, large peak capacities, and reproducible retention times in total ion chromatography (TIC). A total of 19128 ion peaks were detected, and 254 kinds of metabolites were identified in BMSCs. Then, unsupervised multivariate statistics PCA showed that the metabolite profiles were separated among the fluoride-treated groups and control groups (Fig. 5A). Supervised multivariate statistics OPLS-DA and PLS-DA further indicated that the model was reliable, with significant differences being observed between the experimental groups and control groups in both the positive and negative modes. Next, the fragment information obtained from the MS/MS mode was further matched and annotated in online databases to obtain accurate information on metabolites. According to the classification of metabolites in the online KEGG database, the substances were classified as carbohydrates, energy, lipids, nucleotides, amino acids, xenobiotics, peptides, cofactors, and vitamins (Fig. 5B). The hierarchical clustering heatmap presented 20 DAMs (10 upregulated metabolites and 10 downregulated metabolites) based on the criteria of a VIP > 1.0 and $p < 0.05$ (Fig. 5C). The Z score (standard score) was applied to show trends of changes in the relative contents of DAMs in the control and fluoride-treated groups (Fig. 5D). Disturbed metabolic pathways, including glutathione metabolism; D-glutamine and D-glutamate metabolism; and alanine, aspartate, glutamate, arginine, and proline metabolism, are presented in the bubble diagram (Fig. 5E) and were identified in the KEGG pathway analysis. Moreover, the MetPA database in MetaboAnalyst was used to perform a network analysis in which the DAMs were mainly clustered in these metabolic pathways, including D-glutamine and D-glutamate metabolism; alanine, aspartate and glutamate metabolism; and arginine and proline metabolism (Fig. 5F).

3.6. Gene-to-metabolite networks of BMSCs in response to fluoride

To explore the systemic mechanism of fluoride-induced bone toxicity, a total of 197 DEGs and 20 DAMs were subjected to integrated analysis with $p < 0.05$ as determined by the Pearson correlation value, and the correlations and significance among DEGs and DAMs are shown in Fig. S3A. Most of the DEGs were positively correlated with maleic acid, palmitic acid, prostaglandin B2, 15-deoxy-d-12,14-PGJ2 and prostaglandin C2, while pyridoxal phosphate, L-glutamic acid, pyroglutamic acid, L-glutamine and L-lysine were negatively correlated with the DEGs. As shown in Fig. S3B, the altered genes and metabolites were combined to produce integrative signaling networks with Cytoscape (v 3.1.1). Notably, those DAMs and DEGs were mainly clustered in the metabolic pathways of protein digestion and absorption, glutathione metabolism, and mineral absorption. These data are consistent with the results from KEGG pathway enrichment analysis (Figs. S4–6).

3.7. Integrated analysis of lysosomal-related genes and metabolomics data

To investigate biomarkers and metabolic pathways that potentially affect lysosomal function, we further conducted integrated analysis of lysosomal-related genes with DAMs based on the previously reported analytical method. Results indicated that metabolites including palmitic acid, prostaglandin C2 and prostaglandin B2 were positively correlated with the *Atp6v0b* gene, suggesting that these metabolites and the *Atp6v0b* gene are involved in fluoride-induced lysosomal dysfunction in BMSCs (Fig. 6A). Moreover, the contents of palmitic acid, prostaglandin C2 and prostaglandin B2 were increased in 2 mM fluoride-exposed BMSCs compared to the control group as determined by metabolomics profiling (Fig. 6B).

4. Discussion

In our study, we performed *in vitro* experiments and multiomics analysis to explore the toxic effects of fluoride exposure on BMSCs. We found that fluoride reduced the proliferation and survival of BMSCs.

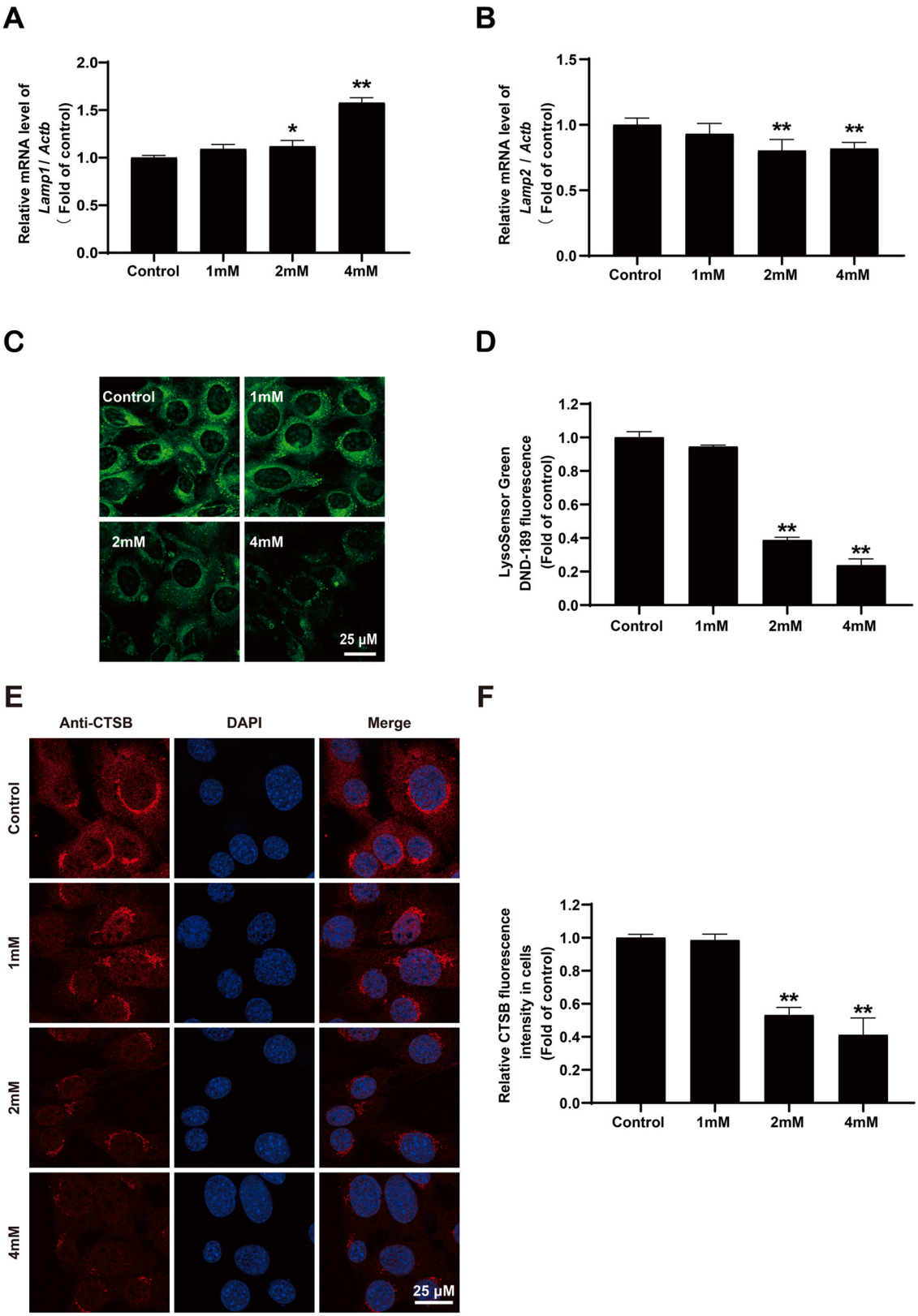

Fig. 3. Fluoride exposure led to lysosomal dysfunction in BMSCs. (A-B) Relative *LAMP 1* and *LAMP 2* mRNA levels in BMSCs treated with fluoride at different concentrations for 24 h. The levels of *LAMP 1* and *LAMP 2* were normalized to the corresponding levels of *ACTB*. (C-D) Representative image of LysoSensor fluorescence staining and quantification of the LysoSensor fluorescence intensity in BMSCs treated with fluoride at different concentrations for 24 h. (E-F) Representative image of CTSB fluorescence staining and quantification of the CTSB fluorescence signaling intensity in BMSCs treated with fluoride at different concentrations for 24 h. The values are presented as the means ± SEM; * $p < 0.05$ and ** $p < 0.01$ versus the control group (n = 4).

A

Table 1 Genes involved in lysosomal pathway from KEGG pathway

Gene ID	Gene Name	log_2 Fold Change	P value
ENSMUSG00000033379	*Atp6v0b*	1.52	0.0278
ENSMUSG00000007038	*Neu1*	1.66	0.0001
ENSMUSG00000035521	*Gnptg*	1.02	0.0084
ENSMUSG00000031266	*Gla*	1.08	0.0023
ENSMUSG00000033540	*Idua*	1.08	0.0274
ENSMUSG00000004567	*Mcoln1*	1.08	0.0350

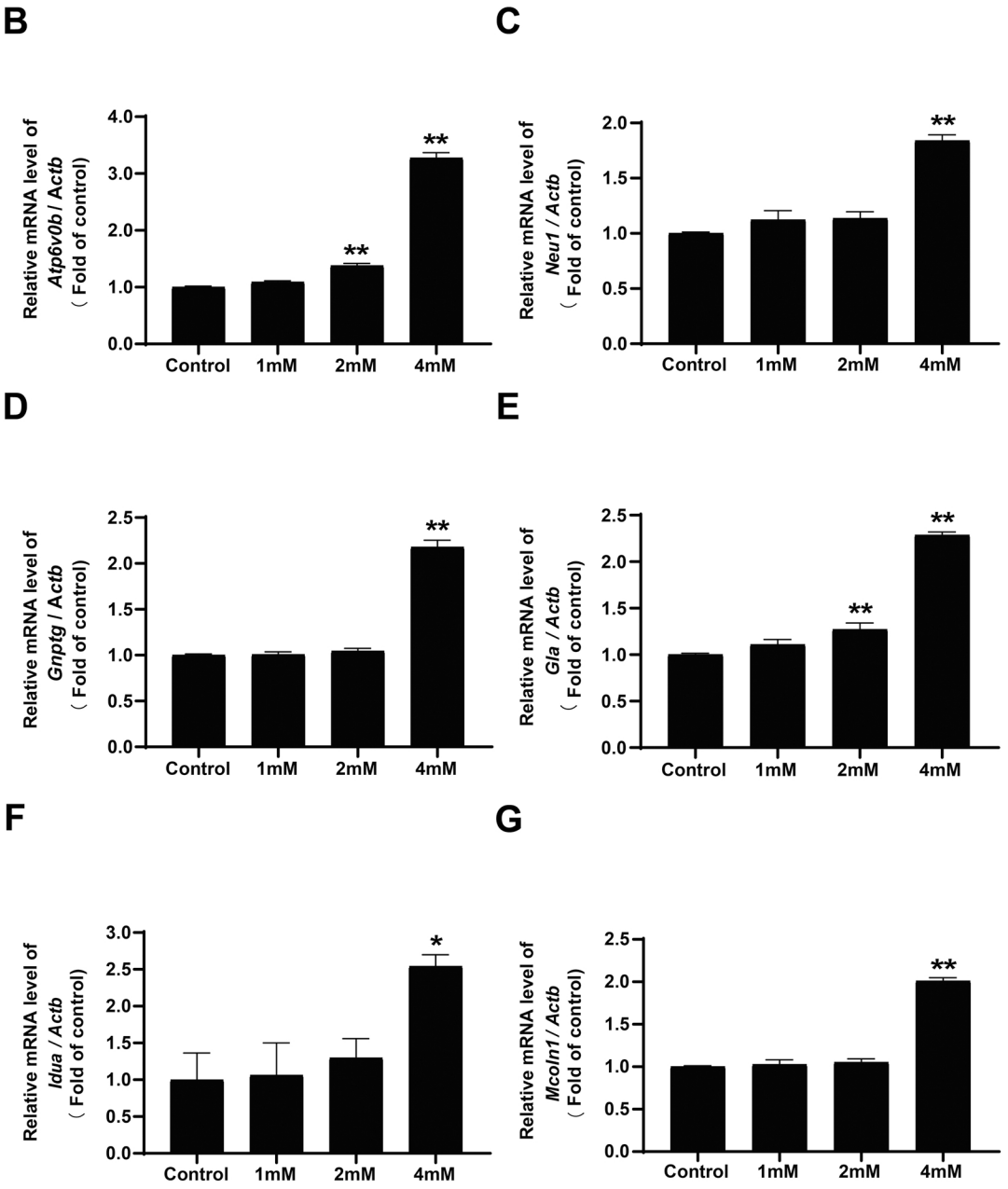

Fig. 4. Fluoride exposure upregulated the expression of *Atp6v0b* and *Gla* in BMSCs. (A) Genes enriched in the lysosome pathway according to the transcriptomic data. (B-G) Relative mRNA levels of *Atp6v0b, Neu1, Gnptg, Gla, Idua,* and *Mcoln1*. The values are presented as the means ± SEM; * $p < 0.05$ and ** $p < 0.01$ versus the control group (n = 4).

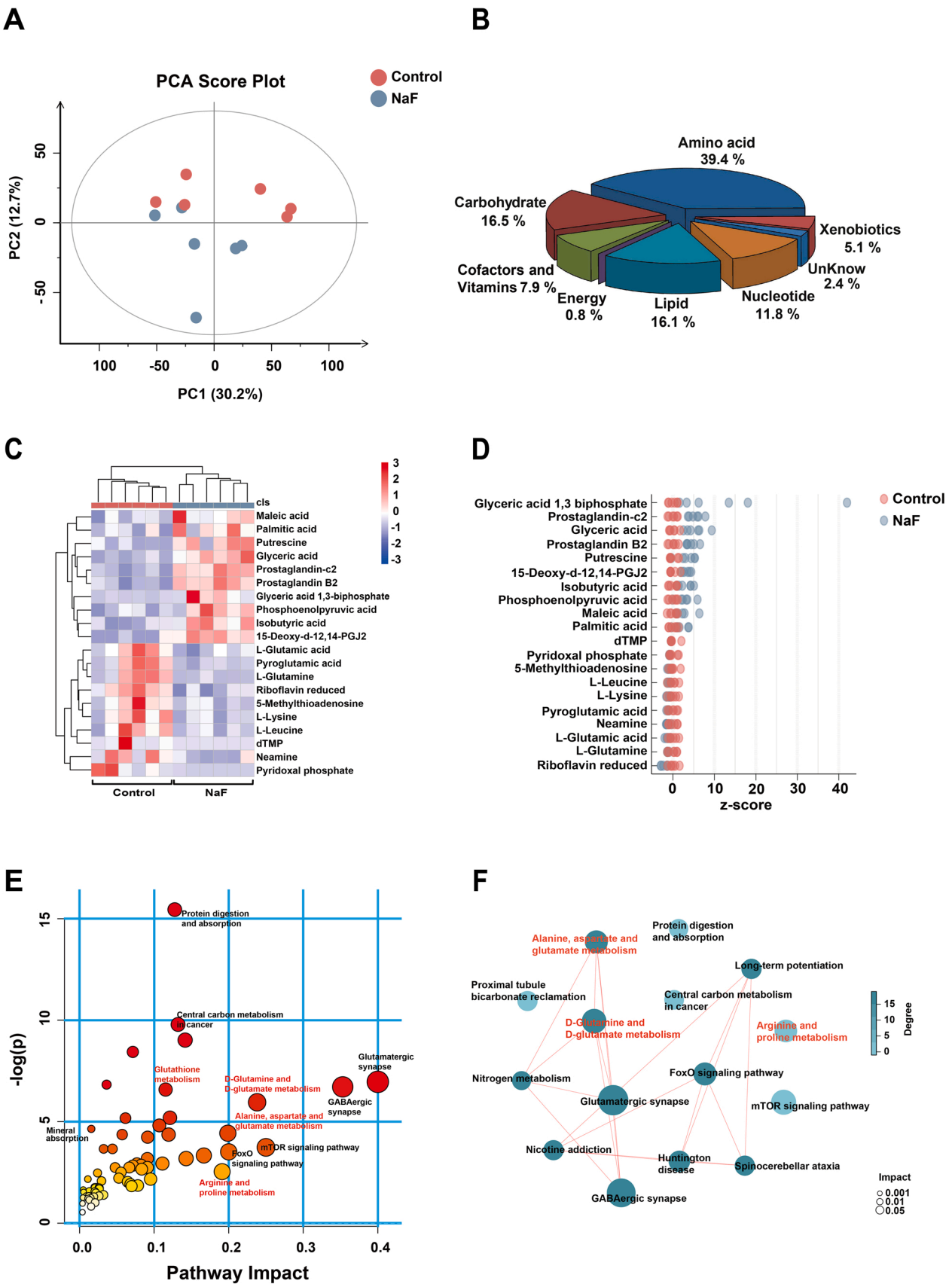

Fig. 5. Fluoride exposure mainly disturbed glutathione metabolism. (A) PCA score plot of the metabolic profiles of the control and 2 mM fluoride-treated groups. (B) Functional classification of total metabolites in BMSCs according to the KEGG database. (C) Heatmap of the hierarchical clustering analysis of 20 DAMs between the control and 2 mM fluoride-treated groups. (D) Z score plot showing the alterations of metabolite contents. (E) Metabolic pathways related to changed metabolites in fluoride-treated BMSCs, as determined using KEGG enrichment analysis. (F) Network diagram of the metabolic pathways in BMSCs exposed to fluoride (n = 6).

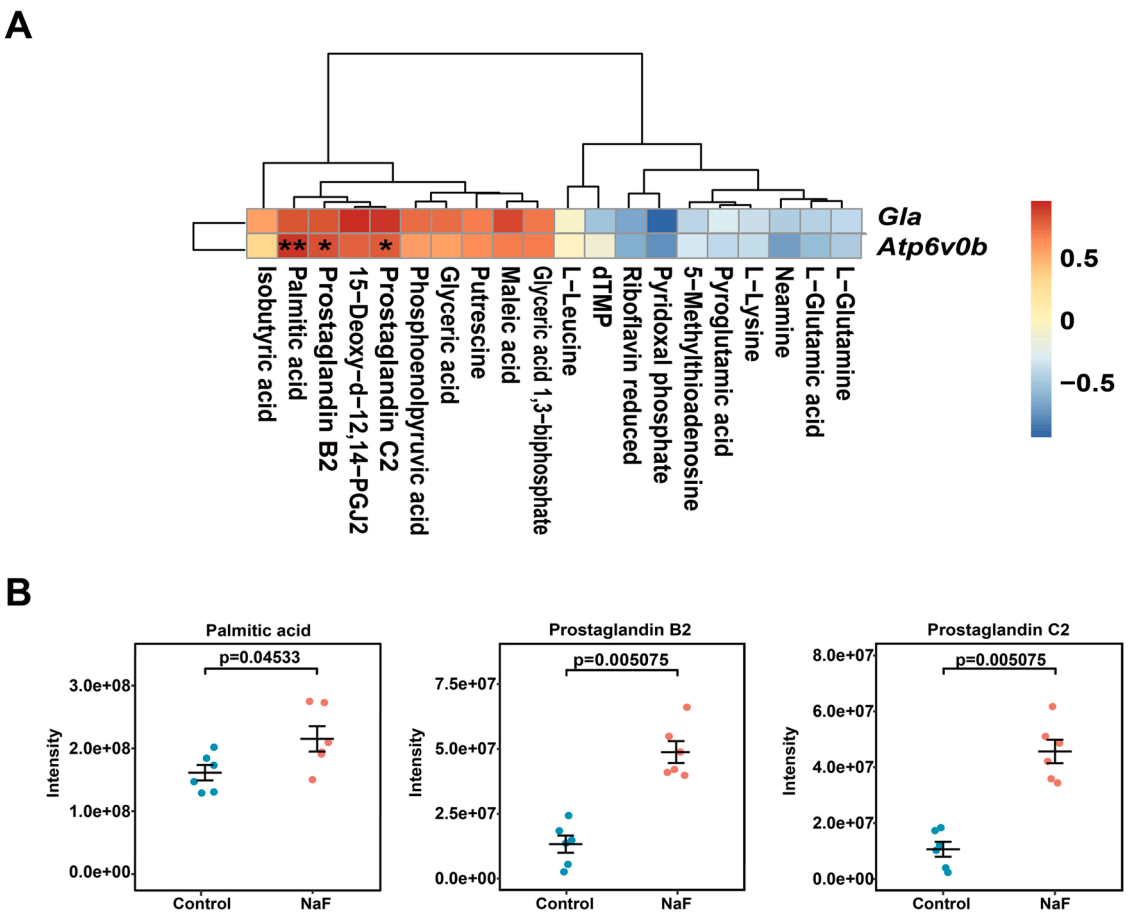

Fig. 6. Alterations in palmitic acid and prostaglandin metabolism were significantly associated with lysosomal function. (A) Clustering analysis heatmap of *Atp6v0b* and DAMs in the metabonomic profiles. (B) Relative intensities of palmitic acid, prostaglandin C2, and prostaglandin B2 in the metabonomic profiles. * $p < 0.05$ and ** $p < 0.01$ versus the control group (n = 6).

Transcriptomics analyses indicated that "lysosome" was the top enriched term in the KEGG pathway analysis. Further experiments demonstrated that fluoride impaired lysosomal function and upregulated genes involved in the lysosomal pathway. Glutathione metabolism was a hub pathway affected in fluoride-exposed BMSCs. Alterations in palmitic acid and prostaglandin metabolism were most significantly associated with the fluoride-induced disruption of lysosomal function, as determined by the validated integrative analysis. These results demonstrated the superiority of multiomics integrative analyses to elucidate toxicity effects and injury mechanisms in fluoride-induced bone toxicity.

The bone toxicity caused by fluoride exposure has become a hot topic over the past twenty years, but the related biological mechanism remains elusive. Due to their high susceptibility to fluoride exposure (Jiang et al., 2020), strong regenerative capacity (Faruk et al., 2021), and potential for differentiation into bone, BMSCs have become an attractive cell model for investigating bone toxicity. Recent studies suggested that the proliferation and survival of BMSCs were substantially reduced after exposure to 32 mg/L (approximately 1.68 mM) fluoride for 7 days (Jiang et al., 2020). Moreover, exposure to 5 mM fluoride for 12 h consistently reduced the viability of BMSCs (Bhawal et al., 2020). Based on previous studies and the IC_{50} of fluoride exposure in our study, we employed BMSCs exposed to 2 mM fluoride, which represented a lower concentration than that used in the aforementioned studies, as a cell model and then utilized multiomics methods to observe the effects and mechanisms of fluoride-induced bone toxicity.

It has been reported that fluoride altered the expression levels of genes involved in biological processes associated with bone development pathways. Likewise, 2632 transcripts associated with oxidative stress, inflammation, osteoblastic differentiation, and bone development pathways were reported to be significantly altered in fluoride-treated HOS cells (Gandhi et al., 2017). Interestingly, our study showed that fluoride exposure resulted in a significant alteration in the expression of genes involved in the ECM-receptor interaction, VEGF signaling pathway, and cell adhesion molecules (CAMs) from the transcriptomic analysis of KEGG pathways. Thus, our finding is consistent with previous studies showing that ECM-receptor interactions, the VEGF signaling pathway, and CAMs are related to osteoblastic differentiation and degradation of the extracellular matrix. Previous studies have documented the pathogenic roles of fluoride in suppressing osteoblast behaviors and promoting degradation of the ECM. In a recent study, chronic fluoride exposure *in vivo* led to histopathological alterations and bone injuries by activating the PI3K/AKT signaling pathway (Wang et al., 2020a, 2020b). Zhu et al. indicated that fluoride inhibited the MAPK/Hippo signaling pathway and reduced the transcriptional activity of the key effector molecule YAP, subsequently decreasing bone strength and impairing bone trabecular structure (Zhu et al., 2019). In our study, the DEGs from transcriptomics profiles were also enriched in these pathways, including ECM-receptor interactions, the Hippo signaling pathway, the MAPK signaling pathway, and the PI3K-Akt signaling pathway. Based on these data, fluoride induced the alteration of these pathways as well as pathway-related genes in BMSCs.

It has been reported that fluoride induced intracellular organelle damage including disruption of mitochondrial membrane integrity (Liang et al., 2020; Zhou et al., 2020), induction of endoplasmic reticulum (ER) stress (Niu et al., 2018; Li et al., 2022) and DNA damage (Fujiwara et al., 2021; Radovanović et al., 2021), as well as interference

with inter-organellar communication or crosstalk (Liang et al., 2020b). Notably, the "lysosome" pathway was the most enriched in the KEGG enrichment pathway transcriptomics analyses in our model. Lysosomes widely exist in eukaryotic cells and sustain intracellular homeostasis by eliminating cellular debris, damaged organelles and invading microorganisms. Recent studies have recognized that fluoride exposure leads to lysosomal dysfunction attributed to dysmorphic morphology containing aggregates and then causes tubulopathy (Rodrigo et al., 2021). Recently, fluoride exposure was shown to affect the expression of piwi-interaction RNAs (piRNAs) and the lysosomal signaling pathway, which led to failure in the fertilization process (Jiang et al., 2019; Li et al., 2021a, 2021b, 2021c, 2021d). Taken together, lysosome is a critical target organelle in fluoride toxicity.

The *LAMP 1/LAMP 2* genes were reported to encode membrane glycoproteins involved in the protection, maintenance, and adhesion of lysosomes (Terasawa et al., 2021). The accumulation of lysosome-like structures or acidic vacuoles, as well as the increased expression of *LAMP 1*, have been reported in fluoride bone toxicity. Consistent with this previous study, we also observed an increase in the expression of the *LAMP 1* gene, further confirming that injured bone cells accumulate lysosomes and lysosome-like structures. CTSB/CTSD were essential proteases that regulated proteolytic activity in the lysosome lumen, and loss of CTSB/CTSD may decrease lysosomal hydrolysis and result in the accumulation of different extracellular proteins implicated in cellular damage (Man and Kanneganti, 2016; Di Spiezio et al., 2021). Moreover, the acidic environment in lysosome provided an optimal microenvironment for various hydrolytic enzymes to facilitate the degradation of proteins and damaged organelles. An increased pH disrupted the acidic environment of the lysosomal lumen, thus affecting the degradation capacity of lysosomes (Liu et al., 2018; Hadi et al., 2021). Han et al. suggested that fluoride exposure elevated the lysosomal pH and diminished CTSD activity and expression, thus reducing the lysosomal degradation capacity (Han et al., 2022). Consistent with the findings mentioned above, our results indicated that fluoride exposure inhibited lysosomal function by decreasing the expression levels of CTSB and increasing the pH in the lysosome lumen. Hence, lysosomal dysfunction is a key factor contributing to fluoride-induced BMSC injury and bone toxicity.

Interestingly, although lysosomal function was compromised after fluoride treatment, the expression of lysosomal-related genes, including *Atp6v0b* and *Gla*, was increased. Studies reported that the *Atp6v0b* gene encoded a component of the proton pump V-ATPase, which consumed ATP and transported hydrogen ions to lysosomes, maintaining acidification in the lysosome lumen (Li et al., 2021a, 2021b, 2021c, 2021d). The evidence supported that fluoride may increase the lysosomal luminal pH by inhibiting the expression of V-ATPase, whereas the fluoride-induced reduction in V-ATPase expression was mitigated by Ad-V-ATPase B2, which ensured the normal acidification of the environment required for the lysosomal degradation process (Han et al., 2022). Surprisingly, *Atp6v0b* expression was upregulated after fluoride exposure in the present study, which may be inconsistent with published findings. Moreover, our previous studies indicated that nuclear translocation of transcription factor EB (TFEB) increased the expression of lysosome-related genes in response to lysosomal stress, which we viewed as a compensatory response to rescue Cd-triggered neurotoxicity (Li et al., 2016; Pi et al., 2017). Therefore, we speculate that upon the fluoride-induced inhibition of lysosome function, MiT/TFE helix-loop-helix subfamily proteins may mobilize into the nucleus and lead to a compensatory lysosomal biogenesis transcriptional response. The elucidation of the mechanistic details requires further research.

Previous studies have indicated significant alterations in serum levels of metabolites, including nicotinamide, adenosine, 1-oleoyl-sn-glycero-3-phosphocholine (OGPC), 1-stearoyl-sn-glycerol 3-phosphocholine (SGPC), urea, betaine and N2-acetyl-L-ornithine, in rats in response to fluoride treatment (Yue et al., 2020). However, our metabonomic profile indicated that the metabolites that are mainly involved in glucose metabolism, glutathione metabolism, and fatty acid metabolism were significantly disturbed in fluoride-treated BMSCs, which may not be fully consistent with the previous study. Because our study was conducted to determine the relationship between fluorosis and metabolites at the cellular level, further *in vivo* verification in an animal model is needed in the future. Fluoride inhibits the activities of enzymes that participate in glycolysis and cellular respiration pathways across various organism models, and most of the metabolites derived from the glycolysis process are disturbed by fluoride exposure (Stapleton et al., 2017; Manome et al., 2019; Maheshwari et al., 2021). Interestingly, in the metabolomic profiles, the increased contents of glyceric acid, 1,3-biphosphate glyceric acid, and phosphoenolpyruvic acid indicated that fluoride may disturb the glycolysis process in BMSCs, which is related to glucose metabolism. Glutathione is a tripeptide composed of glutamic acid, cysteine and glycine and exists in almost every cell in the body to maintain the redox balance via antioxidant and integrated detoxification effects. According to recent findings, fluoride exposure significantly decreases the activities of the antioxidant enzymes glutathione S-transferases (GST), catalase (CAT), superoxide dismutase (SOD), and glutathione peroxidase (GPx), as well as the concentration of the glutathione tripeptide, which may cause imbalances in the cellular redox status in bone tissue (Zheng et al., 2020; Sharma et al., 2021). In addition, fluoride induces the excess production of superfluous reactive oxygen species (ROS) and oxidative stress in BMSCs (Fig. S2), and our findings indicated that fluoride exposure decreased the contents of metabolites that were enriched in the glutathione metabolism pathway, revealing that changes in glutathione metabolism may increase oxidative stress-induced damage in fluoride-treated BMSCs. Additionally, palmitic acid was recently reported to modulate the differentiation, function, and survival of osteoblasts *in vitro*. Studies conducted by Al Saediet et al. revealed that the exposure of osteoblasts to palmitic acid induced autophagy failure and inhibited autophagosome formation, contributing to palmitic acid-induced lipotoxicity (Al Saedi et al., 2019). Consistent with these previous studies, our results also showed that palmitic acid levels were increased by fluoride, suggesting that increased palmitic acid levels may participate in fluoride-triggered BMSC damage. Collectively, the metabolomics results suggest that glycolysis failure in glucose metabolism, glutathione metabolism disorder and the accumulation of palmitic acid in fatty acid metabolism may contribute to BMSC toxicity induced by fluoride exposure.

A set of studies has suggested that fluoride exposure increases cellular dysfunction, which was reversed by different antioxidants. Researchers have concluded that fluoride induces oxidative stress-mediated apoptosis in intestinal epithelial cells by inhibiting glutathione biosynthesis. However, a methanol extract of coconut haustorium improved glutathione biosynthesis to prevent fluoride-induced toxicity in IEC-6 cells by enhancing the enzymatic activity of γ-glutamyl cysteine synthetase (γGCS) and glutathione synthetase (GS) (Job et al., 2021). Moreover, pycnogenol antagonizes fluoride-induced kidney damage by maintaining lysosomal dysfunction *in vivo* (Arhima et al., 2004). Considering the aforementioned findings, glutathione depletion and lysosomal dysfunction in BMSCs may conceivably serve as potential targets for antioxidants to treat fluoride-induced bone toxicity.

A subsequent integrative analysis revealed a possible mechanism of fluoride-induced bone toxicity deserves our attention. Recent studies suggested that palmitic acid induces cell cycle arrest at G2/M phase in hBMSCs via a p53/p21-dependent pathway (Lin et al., 2019). Subsequently, the activated AMPK pathway antagonizes ER stress in hMSCs and cell death induced by palmitate exposure (Lu et al., 2012). In addition, exposure to prostaglandin B2 and prostaglandin C2 is associated with an inflammatory response in MSCs (Van den Berk et al., 2014). In our study, the expression of the lysosome-related gene *Atp6v0b* was positively associated with the DAMs palmitic acid, prostaglandin C2 and prostaglandin B2, which were detected at higher levels after fluoride exposure, indicating that alterations in palmitic acid and prostaglandin metabolism were significantly associated with fluoride-induced

lysosomal dysfunction in BMSCs.

5. Conclusions

In summary, the present study indicated that fluoride exposure disturbed metabolite levels and led to lysosomal dysfunction and bone toxicity in BMSCs. Our study was the first to reveal the toxic effect of fluoride exposure on BMSCs by applying multiomics technology and provided new insights into the mechanism of fluoride-induced bone toxicity. Our findings indicated that fluoride increased the expression levels of genes involved in the lysosomal pathway but led to lysosomal dysfunction and bone toxicity in BMSCs. Subsequently, the metabonomic profile revealed that glutathione metabolism was significantly disturbed in fluoride-treated BMSCs. Notably, the integrative analysis indicated that DAMs, including palmitate, prostaglandin B2, and prostaglandin C2, showed strong correlations with lysosome, which implied potential directions for bone toxicity research using fluoride. Since we did not detect changes in the levels of genes and metabolites *in vivo* in this study, further research should be conducted using fluoride-exposed animal models. The multiomics investigation in the present study supported the hypothesis that fluoride exerts toxicity at the systemic level. Our present study thus highlights the importance of controlling fluoride exposure at the population level.

CRediT authorship contribution statement

Hui Wang, Lu Yang, Peng Gao: Conceptualization, Data curation, Investigation, Methodology, Validation, Writing – original draft. **Ping Deng, Yang Yue, Li Tian, Jia Xie, Mengyan Chen, Yan Luo, Yidan Liang, Weijia Qing**: Data curation, Formal analysis, Validation, Visualization. **Zhou Zhou, Huifeng Pi, Zhengping Yu:** Conceptualization, Formal analysis, Funding acquisition, Project administration, Supervision, Validation, Visualization, Writing – review & editing.

Declaration of Competing Interest

The authors declare that they have no known competing financial interests or personal relationships that could have appeared to influence the work reported in this paper.

Acknowledgments

This work was supported by the National Natural Science Foundation of China (82173473 and 81703267) and the Youth Top-notch Talent Support Program of Chongqing City (CQYC201905014).

Appendix A. Supporting information

Supplementary data associated with this article can be found in the online version at doi:10.1016/j.ecoenv.2022.113672.

References

Abdelhafez, O.H., Othman, E.M., Fahim, J.R., Desoukey, S.Y., Pimentel-Elardo, S.M., Nodwell, J.R., Schirmeister, T., Tawfike, A., Abdelmohsen, U.R., 2020. Metabolomics analysis and biological investigation of three Malvaceae plants. Phytochem. Anal. 31, 204–214.

Affonso, L.N., Marques, J.J., Lima, V., Gonçalves, J.O., Barbosa, S.C., Primel, E.G., Burgo, T., Dotto, G.L., Pinto, L., Cadaval, T.J., 2020. Removal of fluoride from fertilizer industry effluent using carbon nanotubes stabilized in chitosan sponge. J. Hazard. Mater. 388, 122042.

Al Saedi, A., Bermeo, S., Plotkin, L., Myers, D.E., Duque, G., 2019. Mechanisms of palmitate-induced lipotoxicity in osteocytes. Bone 127, 353–359.

Arhima, M.H., Gulati, O.P., Sharma, S.C., 2004. The effect of Pycnogenol on fluoride induced rat kidney lysosomal damage in vitro. Phytother. Res. 18, 244–246.

Bhawal, U.K., Li, X., Suzuki, M., Taguchi, C., Oka, S., Arikawa, K., Tewari, N., Liu, Y., 2020. Treatment with low-level sodium fluoride on wound healing and the osteogenic differentiation of bone marrow mesenchymal stem cells. Dent. Traumatol. 36, 278–284.

Chen, Y.X., Zhu, D.Y., Gao, J., Xu, Z.L., Tao, S.C., Yin, W.J., Zhang, Y.L., Gao, Y.S., Zhang, C.Q., 2019. Diminished membrane recruitment of Akt is instrumental in alcohol-associated osteopenia via the PTEN/Akt/GSK-3β/β-catenin axis. FEBS J. 286, 1101–1119.

Cui, Y., Zhang, B., Ma, J., Wang, Y., Zhao, L., Hou, C., Yu, J., Zhao, Y., Zhang, Z., Nie, J., Gao, T., Zhou, G., Liu, H., 2018. Dopamine receptor D2 gene polymorphism, urine fluoride, and intelligence impairment of children in China: a school-based cross-sectional study. Ecotoxicol. Environ. Saf. 165, 270–277.

Deng, P., Tan, M., Zhou, W., Chen, C., Xi, Y., Gao, P., Ma, Q., Liang, Y., Chen, M., Tian, L., Xie, J., Liu, M., Luo, Y., Li, Y., Zhang, L., Wang, L., Zeng, Y., Pi, H., Yu, Z., Zhou, Z., 2021. Bisphenol A promotes breast cancer cell proliferation by driving miR-381-3p-PTTG1-dependent cell cycle progression. Chemosphere. 268, 129221.

Di Spiezio, A., Marques, A., Schmidt, L., Thießen, N., Gallwitz, L., Fogh, J., Bartsch, U., Saftig, P., 2021. Analysis of cathepsin B and cathepsin L treatment to clear toxic lysosomal protein aggregates in neuronal ceroid lipofuscinosis. Biochim. Biophys. Acta Mol. Basis Dis. 1867, 166205.

Ebrahim, F.M., Nguyen, T.N., Shyshkanov, S., Gładysiak, A., Favre, P., Zacharia, A., Itskos, G., Dyson, P.J., Stylianou, K.C., 2019. Selective, fast-response, and regenerable metal-organic framework for sampling excess fluoride levels in drinking water. J. Am. Chem. Soc. 141, 3052–3058.

Faruk, E.M., Alasmari, W.A., Fouad, H., Nafea, O.E., Hasan, R., 2021. Extracellular vesicles derived from bone marrow mesenchymal stem cells repair functional and structural rat adrenal gland damage induced by fluoride. Life Sci. 270, 119122.

Fujiwara, N., Whitford, G.M., Bartlett, J.D., Suzuki, M., 2021. Curcumin suppresses cell growth and attenuates fluoride-mediated Caspase-3 activation in ameloblast-like LS8 cells. Environ. Pollut. 273, 116495.

Gandhi, D., Naoghare, P.K., Bafana, A., Kannan, K., Sivanesan, S., 2017. Fluoride-induced oxidative and inflammatory stress in osteosarcoma cells: Does it affect bone development pathway? Biol Trace Elem. Res. 175, 103–111.

Geng, N., Ren, X., Gong, Y., Zhang, H., Wang, F., Xing, L., Cao, R., Xu, J., Gao, Y., Giesy, J.P., Chen, J., 2019. Integration of metabolomics and transcriptomics reveals short-chain chlorinated paraffin-induced hepatotoxicity in male Sprague-Dawley rat. Environ. Int. 133, 105231.

Hao, R., Du, X., Yang, C., Deng, Y., Zheng, Z., Wang, Q., 2019. Integrated application of transcriptomics and metabolomics provides insights into unsynchronized growth in pearl oyster Pinctada fucata martensii. Sci. Total Environ. 666, 46–56.

Hadi, M.M., Nesbitt, H., Masood, H., Sciscione, F., Patel, S., Ramesh, B.S., Emberton, M., Callan, J.F., MacRobert, A., McHale, A.P., Nomikou, N., 2021. Investigating the performance of a novel pH and cathepsin B sensitive, stimulus-responsive nanoparticle for optimised sonodynamic therapy in prostate cancer. J. Control Release 329, 76–86.

Han, J., Kiss, L., Mei, H., Remete, A.M., Ponikvar-Svet, M., Sedgwick, D.M., Roman, R., Fustero, S., Moriwaki, H., Soloshonok, V.A., 2021. Chemical aspects of human and environmental overload with fluorine. Chem. Rev. 121, 4678–4742.

Han, X., Tang, Y., Zhang, Y., Zhang, J., Hu, Z., Xu, W., Xu, S., Niu, Q., 2022. Impaired V-ATPase leads to increased lysosomal pH, results in disrupted lysosomal degradation and autophagic flux blockage, contributes to fluoride-induced developmental neurotoxicity. Ecotoxicol. Environ. Saf. 236, 113500.

Helte, E., Donat, V.C., Kippler, M., Wolk, A., Michaëlsson, K., Åkesson, A., 2021. Fluoride in drinking water, diet, and urine in relation to bone mineral density and fracture incidence in postmenopausal women. Environ. Health Perspect. 129, 47005.

Jiang, N., Guo, F., Sun, B., Zhang, X., Xu, H., 2020. Different effects of fluoride exposure on the three major bone cell types. Biol. Trace Elem. Res. 193, 226–233.

Jiang, S., Liang, C., Gao, Y., Liu, Y., Han, Y., Wang, J., Zhang, J., 2019. Fluoride exposure arrests the acrosome formation during spermatogenesis via down-regulated Zpbp1, Spaca1 and Dpy19l2 expression in rat testes. Chemosphere 226, 874–882.

Job, J.T., Rajagopal, R., Alfarhan, A., Ramesh, V., Narayanankutty, A., 2021. Toxic effects of fluoride in intestinal epithelial cells and the mitigating effect of methanol extract of coconut haustorium by enhancing de novo glutathione biosynthesis. Environ. Res. 200, 111717.

Khattak, J.A., Farooqi, A., Hussain, I., Kumar, A., Singh, C.K., Mailloux, B.J., Bostick, B., Ellis, T., van Geen, A., 2022. Groundwater fluoride across the Punjab plains of Pakistan and India: distribution and underlying mechanisms. Sci. Total Environ. 806, 151353.

Li, A., Wang, Y., He, Y., Liu, B., Iqbal, M., Mehmood, K., Jamil, T., Chang, Y.F., Hu, L., Li, Y., Guo, J., Pan, J., Tang, Z., Zhang, H., 2021a. Environmental fluoride exposure disrupts the intestinal structure and gut microbial composition in ducks. Chemosphere 277, 130222.

Li, M., Feng, J., Cheng, Y., Dong, N., Tian, X., Liu, P., Zhao, Y., Qiu, Y., Tian, F., Lyu, Y., Zhao, Q., Wei, C., Wang, M., Yuan, J., Ying, X., Ren, X., Yan, X., 2022. Arsenic-fluoride co-exposure induced endoplasmic reticulum stress resulting in apoptosis in rat heart and H9c2 cells. Chemosphere 288, 132518.

Li, M., Pi, H., Yang, Z., Reiter, R.J., Xu, S., Chen, X., Chen, C., Zhang, L., Yang, M., Li, Y., Guo, P., Li, G., Tu, M., Tian, L., Xie, J., He, M., Lu, Y., Zhong, M., Zhang, Y., Yu, Z., Zhou, Z., 2016. Melatonin antagonizes cadmium-induced neurotoxicity by activating the transcription factor EB-dependent autophagy-lysosome machinery in mouse neuroblastoma cells. J. Pineal. Res. 61, 353–369.

Li, X., Jiang, J., Yang, Z., Jin, S., Lu, X., Qian, Y., 2021b. Galangin suppresses RANKL-induced osteoclastogenesis via inhibiting MAPK and NF-κB signalling pathways. J. Cell. Mol. Med. 25, 4988–5000.

Li, Y., Bi, Y., Mi, W., Xie, S., Ji, L., 2021c. Land-use change caused by anthropogenic activities increase fluoride and arsenic pollution in groundwater and human health risk. J. Hazard. Mater. 406, 124337.

Li, Y., Min, C., Zhao, Y., Wang, J., Wang, J., 2021d. Effects of fluoride on PIWI-interacting RNA expression profiling in testis of mice. Chemosphere 269, 128727.

Liang, C., Gao, Y., He, Y., Han, Y., Manthari, R.K., Tikka, C., Chen, C., Wang, J., Zhang, J., 2020. Fluoride induced mitochondrial impairment and PINK1-mediated mitophagy in Leydig cells of mice: In vivo and in vitro studies. Environ. Pollut. 256, 113438.
Lin, J.H., Ting, P.C., Lee, W.S., Chiu, H.W., Chien, C.A., Liu, C.H., Sun, L.Y., Yang, K.T., 2019. Palmitic acid methyl ester induces G (2)/M arrest in human bone marrow-derived mesenchymal stem cells via the p53/p21 pathway. Stem Cells Int. 2019, 7606238.
Liu, B., Palmfeldt, J., Lin, L., Colaço, A., Clemmensen, K., Huang, J., Xu, F., Liu, X., Maeda, K., Luo, Y., Jäättelä, M., 2018. STAT3 associates with vacuolar H (+)-ATPase and regulates cytosolic and lysosomal pH. Cell Res. 28, 996–1012.
Liu, M., Pi, H., Xi, Y., Wang, L., Tian, L., Chen, M., Xie, J., Deng, P., Zhang, T., Zhou, C., Liang, Y., Zhang, L., He, M., Lu, Y., Chen, C., Yu, Z., Zhou, Z., 2021a. KIF5A-dependent axonal transport deficiency disrupts autophagic flux in trimethyltin chloride-induced neurotoxicity. Autophagy 17, 903–924.
Liu, Y., Liang, Y., Yang, C., Shi, R., Lu, W., Wang, X., Wang, R., Xia, Q., Ma, S., 2021b. A deep insight into the transcriptome of midgut and fat body reveals the toxic mechanism of fluoride exposure in silkworm. Chemosphere 262, 127891.
Liu, Y., Téllez-Rojo, M., Sánchez, B.N., Ettinger, A.S., Osorio-Yáñez, C., Solano, M., Hu, H., Peterson, K.E., 2020a. Association between fluoride exposure and cardiometabolic risk in peripubertal Mexican children. Environ. Int. 134, 105302.
Liu, Y., Yang, Y., Wei, Y., Liu, X., Li, B., Chu, Y., Huang, W., Wang, L., Lou, Q., Guo, N., Wu, L., Wang, J., Zhang, M., Yin, F., Fan, C., Su, M., Zhang, Z., Zhang, X., Gao, Y., Sun, D., 2020b. SKlotho is associated with the severity of brick tea-type skeletal fluorosis in China. Sci. Total Environ. 744, 140749.
Lu, J., Wang, Q., Huang, L., Dong, H., Lin, L., Lin, N., Zheng, F., Tan, J., 2012. Palmitate causes endoplasmic reticulum stress and apoptosis in human mesenchymal stem cells: prevention by AMPK activator. Endocrinology 153, 5275–5284.
Lu, X., Chen, Y., Wang, H., Bai, Y., Zhao, J., Zhang, X., Liang, L., Chen, Y., Ye, C., Li, Y., Zhang, Y., Li, Y., Ma, T., 2019. Integrated lipidomics and transcriptomics characterization upon aging-related changes of lipid species and pathways in human bone marrow mesenchymal stem cells. J. Proteome Res. 18, 2065–2077.
Maheshwari, N., Qasim, N., Anjum, R., Mahmood, R., 2021. Fluoride enhances generation of reactive oxygen and nitrogen species, oxidizes hemoglobin, lowers antioxidant power and inhibits transmembrane electron transport in isolated human red blood cells. Ecotoxicol. Environ. Saf. 208, 111611.
Malin, A.J., Riddell, J., McCague, H., Till, C., 2018. Fluoride exposure and thyroid function among adults living in Canada: Effect modification by iodine status. Environ. Int. 121, 667–674.
Man, S.M., Kanneganti, T.D., 2016. Regulation of lysosomal dynamics and autophagy by CTSB/cathepsin B. Autophagy 12, 2504–2505.
Manome, A., Abiko, Y., Kawashima, J., Washio, J., Fukumoto, S., Takahashi, N., 2019. Acidogenic potential of oral bifidobacterium and its high fluoride tolerance. Front. Microbiol. 10, 1099.
Monnerat, G., Seara, F., Evaristo, J., Carneiro, G., Evaristo, G., Domont, G., Nascimento, J., Mill, J.G., Nogueira, F., Campos, D.C.A., 2018. Aging-related compensated hypogonadism: role of metabolomic analysis in physiopathological and therapeutic evaluation. J. Steroid. Biochem. Mol. Biol. 183, 39–50.
Meena, L., Gupta, R., 2021. Skeletal fluorosis. N. Engl. J. Med. 385, 1510.
Niu, Q., Chen, J., Xia, T., Li, P., Zhou, G., Xu, C., Zhao, Q., Dong, L., Zhang, S., Wang, A., 2018. Excessive ER stress and the resulting autophagic flux dysfunction contribute to fluoride-induced neurotoxicity. Environ. Pollut. 233, 889–899.
Pi, H., Li, M., Tian, L., Yang, Z., Yu, Z., Zhou, Z., 2017. Enhancing lysosomal biogenesis and autophagic flux by activating the transcription factor EB protects against cadmium-induced neurotoxicity. Sci. Rep. 7, 43466.
Pi, H., Li, M., Zou, L., Yang, M., Deng, P., Fan, T., Liu, M., Tian, L., Tu, M., Xie, J., Chen, M., Li, H., Xi, Y., Zhang, L., He, M., Lu, Y., Chen, C., Zhang, T., Wang, Z., Yu, Z., Gao, F., Zhou, Z., 2019. AKT inhibition-mediated dephosphorylation of TFE3 promotes overactive autophagy independent of MTORC1 in cadmium-exposed bone mesenchymal stem cells. Autophagy 15 (4), 565–582.
Qiao, N., Yang, Y., Liao, J., Zhang, H., Yang, F., Ma, F., Han, Q., Yu, W., Li, Y., Hu, L., Pan, J., Hussain, R., Tang, Z., 2021. Metabolomics and transcriptomics indicated the molecular targets of copper to the pig kidney. Ecotoxicol. Environ. Saf. 218, 112284.
Radovanović, J., Antonijević, B., Kolarević, S., Milutinović-Smiljanić, S., Mandić, J., Vuković-Gačić, B., Bulat, Z., Ćurčić, M., Kračun-Kolarević, M., Sunjog, K., Kostić-Vuković, J., Marić, J.J., Antonijević-Miljaković, E., Đukić-Ćosić, D., Djordjevic, A.B., Javorac, D., Baralić, K., Mandinić, Z., 2021. Genotoxicity of fluoride subacute exposure in rats and selenium intervention. Chemosphere 266, 128978.
Rashid, U.S., Bezbaruah, A.N., 2020. Citric acid modified granular activated carbon for enhanced defluoridation. Chemosphere 252, 126639.
Rashid, U.S., Das, T.K., Sakthivel, T.S., Seal, S., Bezbaruah, A.N., 2021. GO-CeO_2 nanohybrid for ultra-rapid fluoride removal from drinking water. Sci. Total Environ. 793, 148547.
Rodrigo, C., Nawarathne, P., Jayasinghe, S., 2021. Chronic interstitial nephritis in agricultural communities (CINAC) and lysosomal tubulopathy: Is there a place for anti-oxidants? Med. Hypotheses 146, 110414.
Shankar, P., Khandare, A.L., Validandi, V., Khandare, S., 2021. Supplementation of calcium and fluoride-free water mitigates skeletal fluorosis in fluoride-intoxicated rats. Biol. Trace Elem. Res. 199, 2225–2237.
Sharma, P., Verma, P.K., Sood, S., Singh, R., Gupta, A., Rastogi, A., 2021. Distribution of fluoride in plasma, brain, and bones and associated oxidative damage after induced chronic fluorosis in wistar rats. Biol. Trace Elem. Res. 200, 1710–1721.
Singh, G., Kumari, B., Sinam, G., Kriti, Kumar, N., Mallick, S., 2018. Fluoride distribution and contamination in the water, soil and plants continuum and its remedial technologies, an Indian perspective- a review. Environ. Pollut. 239, 95–108.
Solanki, Y.S., Agarwal, M., Gupta, A.B., Gupta, S., Shukla, P., 2022. Fluoride occurrences, health problems, detection, and remediation methods for drinking water: a comprehensive review. Sci. Total Environ. 807, 150601.
Stapleton, M., Daly, N., O'Kelly, R., Turner, M.J., 2017. Time and temperature affect glycolysis in blood samples regardless of fluoride-based preservatives: a potential underestimation of diabetes. Ann. Clin. Biochem. 54, 671–676.
Terasawa, K., Kato, Y., Ikami, Y., Sakamoto, K., Ohtake, K., Kusano, S., Tomabechi, Y., Kukimoto-Niino, M., Shirouzu, M., Guan, J.L., Kobayashi, T., Iwata, T., Watabe, T., Yokoyama, S., Hara-Yokoyama, M., 2021. Direct homophilic interaction of LAMP 2A with the two-domain architecture revealed by site-directed photo-crosslinks and steric hindrances in mammalian cells. Autophagy 17, 4286–4304.
Van den Berk, L.C., Jansen, B.J., Snowden, S., Siebers-Vermeulen, K.G., Gilissen, C., Kögler, G., Figdor, C.G., Wheelock, C.E., Torensma, R., 2014. Cord blood mesenchymal stem cells suppress DC-T cell proliferation via prostaglandin B2. Stem Cells Dev. 23, 1582–1593.
Wang, J., Xu, H., Cheng, X., Yang, J., Yan, Z., Ma, H., Zhao, Y., Ommati, M.M., Manthari, R.K., Wang, J., 2020a. Calcium relieves fluoride-induced bone damage through the PI3K/AKT pathway. Food Funct. 11, 1155–1164.
Wang, M., Liu, L., Li, H., Li, Y., Liu, H., Hou, C., Zeng, Q., Li, P., Zhao, Q., Dong, L., Zhou, G., Yu, X., Liu, L., Guan, Q., Zhang, S., Wang, A., 2020b. Thyroid function, intelligence, and low-moderate fluoride exposure among Chinese school-age children. Environ. Int. 134, 105229.
Wang, Y., Li, A., Mehmood, K., Hussain, R., Abbas, R.Z., Javed, M.T., Chang, Y.F., Hu, L., Pan, J., Li, Y., Shi, L., Tang, Z., Zhang, H., 2021. Long-term exposure to the fluoride blocks the development of chondrocytes in the ducks: The molecular mechanism of fluoride regulating autophagy and apoptosis. Ecotoxicol. Environ. Saf. 217, 112225.
Wei, W., Pang, S., Sun, D., 2019. The pathogenesis of endemic fluorosis: Research progress in the last 5 years. J. Cell. Mol. Med. 23, 2333–2342.
Yang, M., Pi, H., Li, M., Xu, S., Zhang, L., Xie, J., Tian, L., Tu, M., He, M., Lu, Y., Yu, Z., Zhou, Z., 2016. From the cover: autophagy induction contributes to cadmium toxicity in mesenchymal stem cells via AMPK/FOXO3a/BECN1 signaling. Toxicol. Sci. 154, 101–114.
Yu, F.F., Zuo, J., Fu, X., Gao, M.H., Sun, L., Yu, S.Y., Li, Z., Zhou, G.Y., Ba, Y., 2021. Role of the hippo signaling pathway in the extracellular matrix degradation of chondrocytes induced by fluoride exposure. Ecotoxicol. Environ. Saf. 225, 112796.
Yue, B., Zhang, X., Li, W., Wang, J., Sun, Z., Niu, R., 2020. Fluoride exposure altered metabolomic profile in rat serum. Chemosphere 258, 127387.
Yue, Y., Deng, P., Xiao, H., Tan, M., Wang, H., Tian, L., Xie, J., Chen, M., Luo, Y., Wang, L., Liang, Y., Pi, H., Zhou, Z., Yu, Z., 2021. N6-methyladenosine-mediated downregulation of miR-374c-5p promotes cadmium-induced cell proliferation and metastasis by targeting GRM3 in breast cancer cells. Ecotoxicol. Environ. Saf. 229, 113085.
Zhang, J., Jiang, N., Yu, H., Yu, X., Guo, F., Zhao, Z., Xu, H., 2019. Requirement of TGFβ signaling for effect of fluoride on osteoblastic differentiation. Biol. Trace Elem. Res. 187, 492–498.
Zhao, W.P., Wang, H.W., Liu, J., Zhang, Z.H., Zhu, S.Q., Zhou, B.H., 2019. Mitochondrial respiratory chain complex abnormal expressions and fusion disorder are involved in fluoride-induced mitochondrial dysfunction in ovarian granulosa cells. Chemosphere 215, 619–625.
Zheng, B., Shi, C., Muhammed, F.K., He, J., Abdullah, A.O., Liu, Y., 2020. Gastrodin alleviates bone damage by modulating protein expression and tissue redox state. FEBS Open Bio. 10, 2404–2416.
Zhou, B.H., Wei, S.S., Jia, L.S., Zhang, Y., Miao, C.Y., Wang, H.W., 2020. Drp1/Mff signaling pathway is involved in fluoride-induced abnormal fission of hepatocyte mitochondria in mice. Sci. Total Environ. 725, 138192.
Zhu, W.Q., Yu, Y.J., Xu, L.N., Ming, P.P., Shao, S.Y., Qiu, J., 2019. Regulation of osteoblast behaviors via cross-talk between Hippo/YAP and MAPK signaling pathway under fluoride exposure. J. Mol. Med. (Berl) 97, 1003–1017.
Zou, Q., Hong, W., Zhou, Y., Ding, Q., Wang, J., Jin, W., Gao, J., Hua, G., Xu, X., 2016. Bone marrow stem cell dysfunction in radiation-induced abscopal bone loss. J. Orthop. Surg. Res. 11, 3.